Loss of time-delay signature in a ring of three unidirectionally coupled semiconductor lasers

Lei Yang (杨 磊)*, Wei Pan (潘 炜), Lianshan Yan (闫连山), Bin Luo (罗 斌), Penghua Mu (穆鹏华), and Nianqiang Li (李念强)

Center for Information Photonics & Communications, School of Information Science and Technology, Southwest Jiaotong University, Chengdu 610031, China

**Corresponding author: yanglei19811212@gmail.com*

Received December 12, 2014; accepted January 16, 2015; posted online March 10, 2015

A ring of three unidirectionally coupled semiconductor lasers (RTUC-SLs) is used to generate broadband chaos with no pronounced time-delay (TD) signature. Using the autocorrelation function and permutation entropy as the TD measures, we demonstrate that under suitable coupling strength, the loss of the TD signature of the lasers in the RTUC-SL configuration is achieved both for the intensity and the phase. These findings should prove valuable for developing high-quality optical chaos for potential applications, such as chaos-based communications and random number generation.

OCIS codes: 140.5960, 190.3100.
doi: 10.3788/COL201513.041403.

Nonlinear dynamics in chaotic semiconductor lasers (SLs) have attracted great interest[1], giving rise to a flurry of reporting about potential applications in secure communications[2,3], chaotic lidar/radar[4], random number generation[5–9], and so on. It is well accepted that the optical chaos generated by laser diodes can enhance the performance of these aforementioned applications. Recently, there has also been considerable interest expressed in the identification or concealment of time-delay (TD) signatures in chaotic SLs with optical injection or delayed feedback[10–16]. In fact, the presence of such TD signatures should be considered as a flaw of the chaotic signals, because it compromises the security of chaos-based communications, as well as limits the choices of sampling periods in random number generation. In all of these considerations, there is the need to eliminate or at least suppress the information about the TD extracted from chaotic waveforms.

The existing theoretical and experimental studies have demonstrated that the loss of the TD signature could be realized with a single chaotic SL[17–19], mutually coupled SLs[20–23], a solitary SL subject to chaotic injection[24,25], or cascaded-coupled SLs[26]. It has been proven that digital keys can be used to suppress the delay signature in chaotic dynamics[27]. Very recently, the role of the phase in TD identification has been emphasized[23,28]. For example, in a chaotic SL subject to optical feedback, it has been suggested that the TD can be concealed in the intensity time series when the feedback delay is chosen so that it is close to the relaxation period of the SL with moderate feedback[10,11]. However, it has been theoretically demonstrated that the TD signature could be readily identified from the phase time series[28], which intuitively degrades the system's performance. Therefore, it is of vital importance to hide the TD signature from both the intensity and phase time series.

Here, we demonstrate that a ring of three unidirectionally coupled SLs (RTUC-SLs) can be used to suppress the TD signature in both the intensity and phase time series simply through the proper choice of the coupling strength. This suppression results from a complex nonlinear interaction between the lasers (active devices) in the RTUC-SLs configuration. Moreover, the TD signature computed from the intensity time series is found to increase as the feedback strength increases. This system provides a concrete physical platform to study the role of control parameters in changing the TD signature, and should therefore provide an additional avenue to be used in the generation of low TD signature chaos. Furthermore, although it is a more complex system in comparison with a single SL, the proposed RTUC-SLs could be easy to implement in photonic integrated circuits[29,30], thereby allowing chaos generation with a TD signature that is well concealed for important applications, such as secure communications.

The schematic diagram for the RTUC-SLs system is shown in Fig. 1. This configuration has been studied for other purposes[31,32]. Note that three SLs are unidirectional-coupled in a ring configuration, which is achieved with the help of isolators. SL1 is unidirectionally

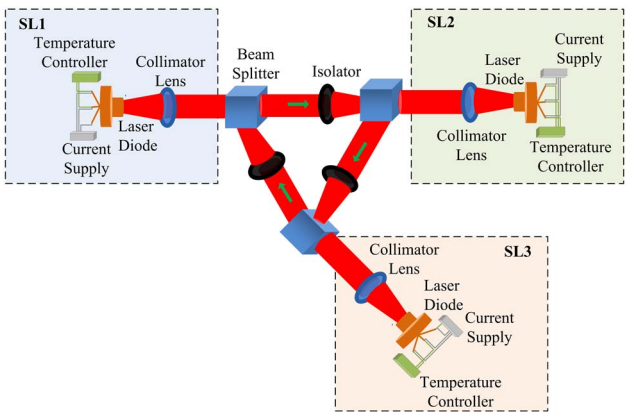

Fig. 1. Schematic of a RTUC-SLs system.

injected into SL2, then SL2 is unidirectionally injected into SL3, and SL3 closes the loop by injecting a proportion of its chaotic output into SL1. Under the proper circumstances, the three SLs operate in a chaotic regime. The simulations are carried out based on their chaotic outputs.

The model equations for the complex, slowly varying envelope of the electric field $E(t)$ and the carrier number inside the cavity $N(t)$ can be derived from the well-known Lang and Kobayashi model. Taking into account the unidirectional coupling effect, the equations of the RTUC-SLs are written as[31,32]

$$\dot{E}_m(t) = \frac{1}{2}(1+i\alpha)\left[\frac{g(N_m(t)-N_0)}{1+s|E_m(t)|^2} - \frac{1}{\tau_p}\right]E_m(t) + \gamma E_k\left(t-\frac{\tau}{3}\right)\exp\left(-i\frac{\omega\tau}{3}\right), \quad (1)$$

$$\dot{N}_m(t) = \frac{J_m}{e} - \frac{N_m(t)}{\tau_s} - \frac{g(N_m(t)-N_0)}{1+s|E_m(t)|^2}|E_m(t)|^2, \quad (2)$$

where the index $m, k = 1, 2, 3$ stands for the laser number, and only three pairs, $(m, k) = (1, 3)$, $(m, k) = (2, 1)$, and $(m, k) = (3, 2)$ are considered in Eq. (1). Parameter $\alpha = 5$ is the linewidth enhancement factor, $g = 1.5 \times 10^{-8}$ ps^{-1} is the differential gain coefficient, $N_0 = 1.5 \times 10^8$ is the carrier number at transparency, $s = 10^{-7}$ is the gain saturation coefficient, $\tau_p = 2$ ps is the photon lifetime, $\tau_s = 2$ ns is the carrier lifetime, and e is the electron charge. $J_m = 2J_{\text{th}}$ is the pump current ($J_{\text{th}} = 14.7$ mA is the threshold current), $\tau = 6$ ns is the total delay of the ring loop, $\omega\tau/3$ is the phase of the injected field ($\omega = 1.216 \times 10^{15}$ rad/s is the angular frequency of the free-running SL), and γ denotes the coupling strength and will be varied in the simulations. For simplicity, the three SLs are assumed to have the same parameters. The influences of the spontaneous emission noise and the frequency detuning are neglected in this work.

Many statistical methods have been designed to identify the TD signature. Well-known methods include autocorrelation function (ACF), delayed mutual information (DMI), filling factor, extreme statistics and permutation entropy (PE)[10,11,15,33–35]. Here, ACF and PE were adopted to retrieve the TD signature, due to the fact that the two measures are substantially resistant to noise, and are computationally efficient.

The ACF $[C(\Delta t)]$ that measures how well the time series matches its time-shifted version is defined as[11]

$$C(\Delta t) = \frac{\langle (I(t+\Delta t) - \langle I(t)\rangle)(I(t) - \langle (t)\rangle)\rangle}{(\langle I(t+\Delta t) - \langle I(t+\Delta t)\rangle\rangle^2 \langle I(t) - \langle I(t)\rangle\rangle^2)^{1/2}}, \quad (3)$$

where $I(t) = |E(t)|^2$ is the intensity time series and $I(t+\Delta t)$ contains the time shift Δt with respect to $I(t)$. Note that the ACF can also be applied to the phase time series.

PE, which is a complement method to the ACF and the DMI, is derived from the information theory. According to Refs. [34–37], one can find the following formulas of PE by first generating an ordinal pattern such as

$$X_i\ (x_{i-(D_x-1)\tau_e}, x_{i-(D_x-2)\tau_e}, ..., x_{i-\tau_e}, x_i), \quad (4)$$

where $D_x \in \mathrm{N}^+$ ($\tau_e \in \mathrm{N}^+$) is the embedding dimension (delay) when a time series $\{x_t, t = 1, ..., N\}$ is given. Then, each time i occurs, we assign a D_x-dimensional vector that results from the evaluation of the time series at times $i-(D_x-1)\tau_e, ..., i-\tau_e, i$. By the ordinal pattern of D_x related to the time i, one can define $x_{i-r_{D_x-1}\tau_e} \le x_{i-r_{D_x-2}\tau_e} \le ... \le x_{i-r_1\tau_e} \le x_{i-r_0\tau_e}$. Then, a unique permutation $\hat{x}_i = (r_0, r_1, ..., r_{D_x-1})$ of $(0, 1, ..., D_x-1)$ is obtained. In this way, any vector X_i is converted into a unique symbol $\hat{x}_i$. For all of the possible $D_x!$ permutations, the associated relative frequencies are defined by

$$p(\hat{x}_i) = \frac{\#\{i | 1+(D_x-1)\tau_e \le i \le N, i \text{ has type } \hat{x}_i\}}{N-(D_x-1)\tau_e}, \quad (5)$$

where # means "number." The PE is calculated based on the relative frequencies of the ordinal patterns, i.e., $H[P] = -\Sigma p(\hat{x}_i)\log\, p(\hat{x}_i)/\log(D_x!)$. Throughout this Letter, the numerical simulations of Eqs. (1)–(3) are performed by using a fourth-order Runge–Kutta algorithm, where the sample period is $\Omega_s = 1$ ps and the sampled time series contains 5000 data points. By fixing $D_x(= 5)$ and varying τ_e, one obtains a PE curve versus $\tau_d(= \tau_e \times \Omega_s)$, where the TD signature is identified in terms of sharp and well-defined minimums.

The lasers in such a RTUC-SLs configuration display a quasi-periodic route to chaos, as shown in the bifurcation diagram of Fig. 3(a) in Ref. [31]. It can be seen that when the feedback strength is low, the lasers oscillate periodically due to the higher coupling strength quasi-periodicity that is taking place. By means of three Hopf bifurcations, the lasers output chaos.

Figure 2 represents a typical example of the intensity time series, ACF curves, PE curves, and power spectra for the three lasers when $\gamma = 20$ ns^{-1}. The intensity time series [Figs. 2(a1)–2(c1)] exhibits a noise-like behavior and consists of complex fluctuations with large amplitude (here, it is rescaled to the magnitude of 10^6). Interestingly, the ACF [Figs. 2(a2)–2(c2)] and PE [Figs. 2(a3)–2(c3)] curves show no obvious TD signature. By calculating the cross-correlation defined in[3], one can confirm that, with the chosen γ, the correlation between any two lasers is relatively low (~0.2), such that all of them can be regarded as chaotic sources.

To gain more insight into the concealment of the TD signature computed from the intensity time series in the RTUC-SLs, TD signature evolution maps of the lasers were plotted when γ varies from 15 to 150 ns^{-1}. The results for SL1, SL2, and SL3 are shown in Fig. 3. By comparison, the ACF maps for the three lasers show similar behaviors. For low and moderate γ values (about

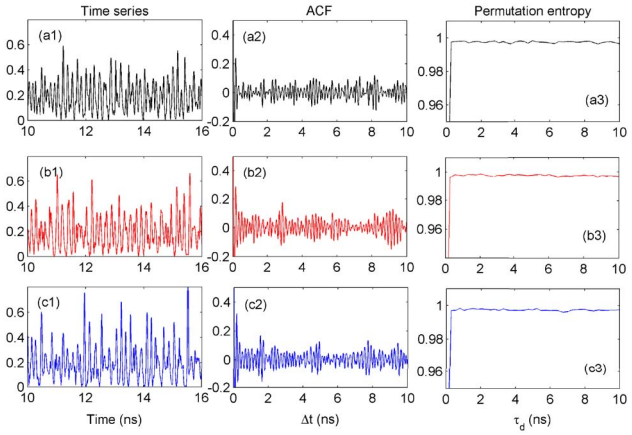

Fig. 2. Intensity time traces (first column), ACF curves (second column), PE (third column). (a1)–(a3) correspond to SL1, (b1)–(b3) correspond to SL2, and (c1)–(c3) correspond to SL3.

from 15 to 50 ns^{-1}), the lasers show an almost completely suppressed TD signature, whereas it becomes more pronounced for higher γ values. In particular, one can see that as γ is increased from 15 to 150 ns^{-1}, the TD signature of the lasers gradually increases. Moreover, the ACF curves and PE curves are presented in Fig. 3 when $\gamma = 15, 30$, and 80 ns^{-1}, which confirms the ACF maps of the lasers. Such TD behaviors were also observed in mutually coupled SLs[22], since a ring with N elements and two bi-directionally coupled SLs possess similar scaling behavior from their correlation properties[27,38]. The concealment of the TD signature in the RTUC-SLs can be attributed to the same physical reason: the laser is an active nonlinear device and responds differently to the input chaotic signal for different coupling parameters. Thus, the periodicity feature due to the coupling delay may be removed. The proposed ring configuration further improves such behavior, which is beneficial to the TD signature suppression.

When motivated by a significant phenomenon, the TD signature can be well concealed from the phase time series in semiconductor ring lasers with cross-feedback[18] and mutually-coupled SLs[23]. We further explore whether it is possible to conceal the TD signature in the phase time series. Figure 4 shows the TD signature evolution maps of the lasers computed from the phase time series when γ is varied from 15 to 150 ns^{-1}. It is of great interest to find that there exists no pronounced peak for the γ values considered, which differs from those in Fig. 3. Even when γ is set to 80 ns^{-1}, one can only observe an ACF peak of a relatively weak level around $\tau = 6$ ns, as shown in Figs. 4(c1), 4(f1), and 4(i1). This indicates that the RTUC-SLs configuration might be a desired chaos generator, at least if it operates in a regime where no obvious TD signature exists for the intensity and phase time series.

In the following, we investigate the influence of γ on the ACF peak computed from the intensity, the phase, and from the real Re$[E(t)]$ and imaginary Im$[E(t)]$ parts of the electric field. Here, the ACF peak (the most pronounced peak) around the coupling delay $\tau = 6$ ns was searched, i.e., $\Delta t \in [-5.5, 6.5]$ ns. The results for the three lasers are shown in Fig. 5. We see that the curve of the ACF peak computed from the intensity increases with increasing γ, despite the fact that there is a certain fluctuation. Contrarily, the curves computed from other observables tend to keep constant around a very weak level (almost below 0.1) as γ increases, which is a benefit

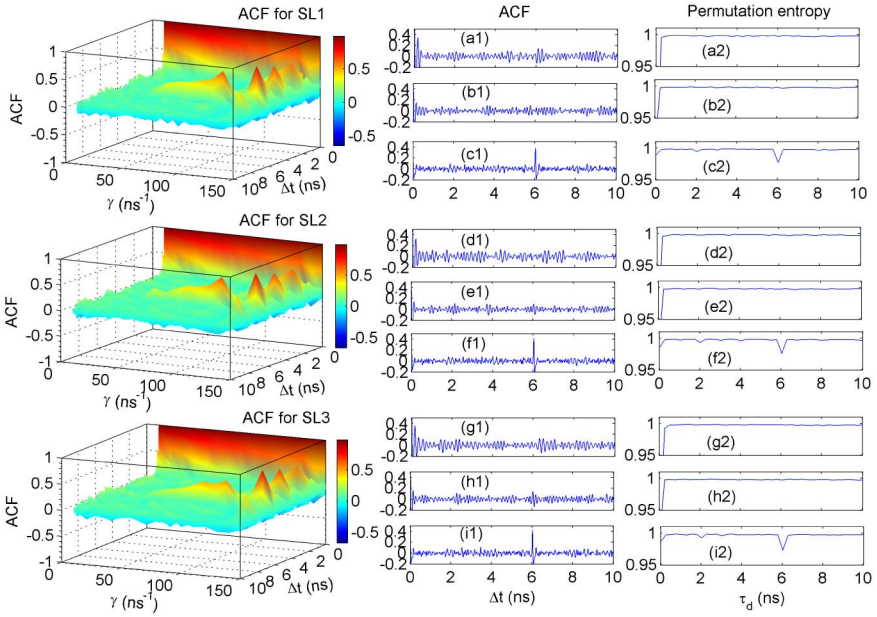

Fig. 3. ACF curves evolution (left column) of the intensity time series in the RTUC-SLs when $\gamma \in [15, 150]$ ns^{-1}. The ACF (middle column) and PE (right column) curves of each laser for $\gamma = 15$, 30, and 80 ns^{-1} (from top to bottom for each laser) are presented for comparison.

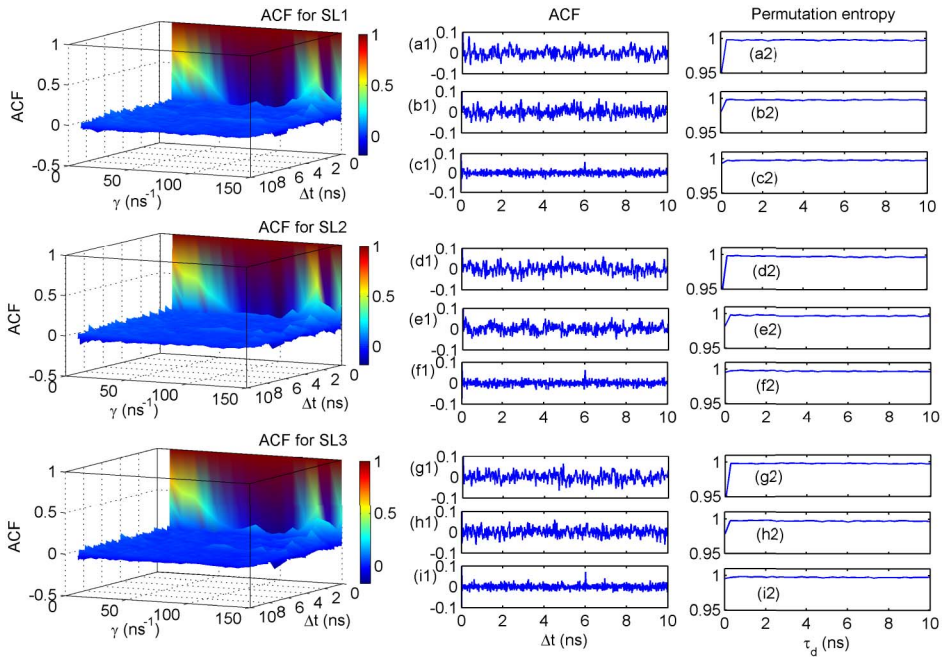

Fig. 4. The evolution of the ACF curves (left column) of the phase time series in a RTUC-SLs when $\gamma \in [15, 150]$ ns^{-1}. The ACF (middle column) and PE (right column) curves of each laser for $\gamma = 15$, 30, and 80 ns^{-1} (from top to bottom for each laser) are presented for comparison.

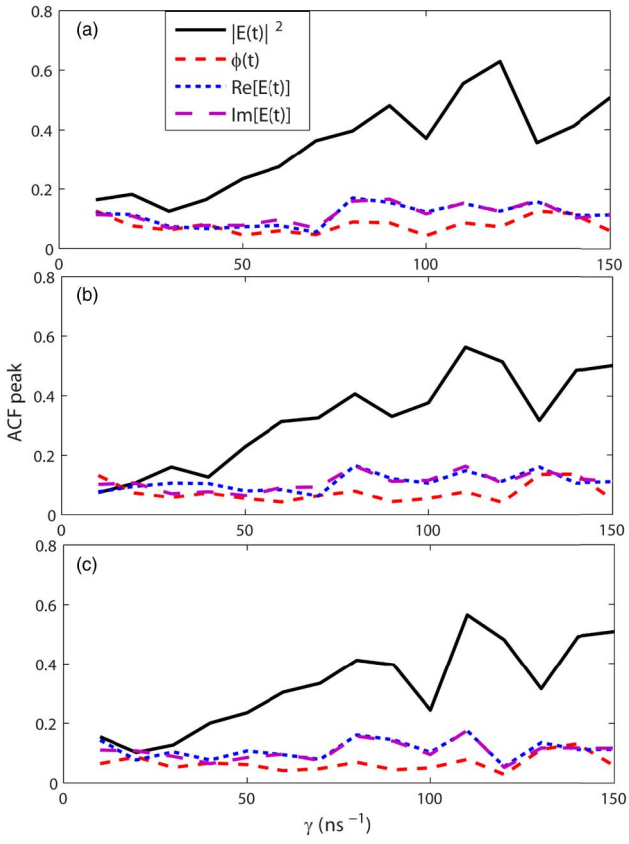

Fig. 5. The ACF peak versus γ, where the results for the intensity ($|E(t)|^2$), phase ($\phi(t) = \mathrm{Arg}[E(t)]$), real ($\mathrm{Re}[E(t)]$), and imaginary ($\mathrm{Im}[E(t)]$) parts of the complex field are contained. (a) corresponds to SL1, (b) corresponds to SL2, and (c) corresponds to SL3.

from the specific ring configuration as explained above. Figure 5 also confirms that a similar tendency can be obtained for the three lasers.

If γ is increased to a critical value, the injection locking appears, giving rise to a different TD signature, as illustrated in the insets of Fig. 6. When $\gamma = 120$ ns^{-1}, in addition to the peak around $\Delta t = 6$ ns, the ACF curve also shows obvious peaks around the sub-harmonics of the coupling delay for large γ values, i.e., $\Delta t = 2$ and 4 ns. When γ is further increased to 160 ns^{-1}, the ACF peak around $\Delta t = 2$ ns becomes most pronounced. The reason can be explained as follows. For higher γ values, the lasers become almost synchronized. When one laser is injected

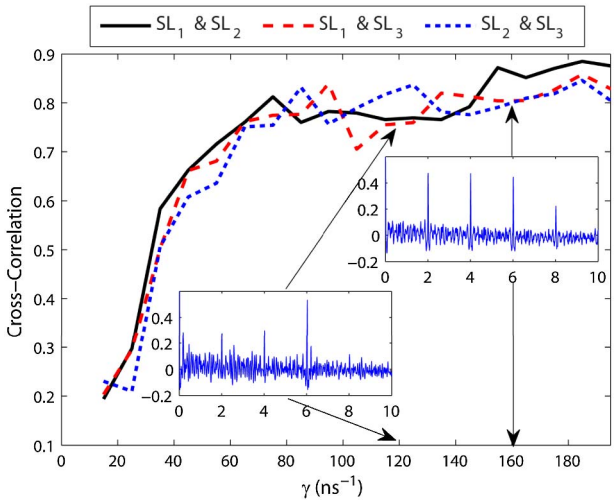

Fig. 6. Cross-correlation between two lasers versus γ. The insets present the ACF curves for $\gamma = 120$ and 150 ns^{-1}.

into another laser, the latter has the ability to reproduce the chaotic fluctuations injected from the former due to the strong injection-locking effect. Because the flight time between two lasers is 2 ns (= 6/3 ns), each laser receives the "self-copy," which is only delayed by 2 ns. This produces the most obvious ACF peak around $\Delta t = 2$ ns. Furthermore, Fig. 6 also shows the cross-correlation versus γ for the lasers. A comparison between Figs. 5 and 6 shows that one can obtain high-quality chaos with TD signature suppression when γ is smaller than 40 ns^{-1}. Meanwhile, the outputs of the lasers in the RTUC-SLs system exhibit low correlation (with the cross-correlation being well below 0.4).

In conclusion, we propose a RTUC-SLs configuration for broadband chaos generation with a TD signature that is well concealed. The influence of the coupling strength on the loss of the TD signature is investigated. By selecting the proper choice of the coupling strength, the RTUC-SLs allow for the concealment of the TD signature in both intensity and phase. This indicates that such a ring configuration might be a desirable chaos generator for applications of interest. A more systematic analysis of the influence of the injection parameters, i.e., coupling strength and frequency detuning, on the TD signature can be the subject of further studies. In addition, our findings may motivate a similar study on a RTUC chaotic two-component electronic circuits[39].

This work was supported by the National Natural Science Foundation of China (61274042).

References

1. M. C. Soriano, J. García-Ojalvo, C. R. Mirasso, and I. Fischer, Rev. Mod. Phys. **85**, 421 (2013).
2. A. Argyris, D. Syvrids, L. Larger, V. A. Lodi, P. Colet, I. Fischer, J. G. Ojalvo, C. R. Mirasso, L. Pesquera, and K. A. Shore, Nature **438**, 343 (2005).
3. I. S. Amiri and J. Ali, Chin. Opt. Lett. **11**, 041901 (2013).
4. F. Y. Lin and J. M. Liu, IEEE J. Sel. Top. Quantum Electron. **10**, 991 (2004).
5. A. Uchida, K. Amano, M. Inoue, K. Hirano, S. Naito, H. Someya, I. Oowada, T. Kurashige, M. Shiki, S. Yoshimori, K. Yoshimura, and P. Davis, Nat. Photonics **2**, 728 (2008).
6. I. Reidler, Y. Aviad, M. Rosenbluh, and I. Kanter, Phys. Rev. Lett. **103**, 024102 (2009).
7. I. Kanter, Y. Aviad, I. Reidler, E. Cohen, and M. Rosenbluh, Nat. Photonics **4**, 58 (2010).
8. X. Z. Li and S. C. Chan, Opt. Lett. **37**, 2163 (2012).
9. X. Z. Li and S. C. Chan, IEEE J. Quantum Electron. **49**, 829 (2013).
10. D. Rontani, A. Locquet, M. Sciamanna, and D. S. Citrin, Opt. Lett. **32**, 2960 (2007).
11. D. Rontani, A. Locquet, M. Sciamanna, D. S. Citrin, and S. Ortin, IEEE J. Quantum Electron. **45**, 879 (2009).
12. S. S. Li, Q. Liu, and S. C. Chan, IEEE Photon. J. **4**, 1930 (2012).
13. S. Priyadarshi, Y. H. Hong, I. Pierce, and K. A. Shore, IEEE J. Sel. Top. Quantum Electron. **19**, 1700707 (2013).
14. S. Y. Xiang, W. Pan, L. Y. Zhang, A. J. Wen, L. Shang, H. X. Zhang, and L. Lin, Opt. Commun. **324**, 38 (2014).
15. Y. Guo, Y. Wu, and Y. Wang, Chin. Opt. Lett. **10**, 061901 (2012).
16. Y. Wu, Y. C. Wang, P. Li, A. B. Wang, and M. J. Zhang, IEEE J. Quantum Electron. **48**, 1371 (2012).
17. J. Hizanidis, S. Deligiannidis, A. Bogris, and D. Syvridis, IEEE J. Quantum Electron. **46**, 1642 (2010).
18. R. M. Nguimdo, G. Verschaffelt, J. Danckaert, and G. V. D. Sande, Opt. Lett. **37**, 2541 (2012).
19. A. B. Wang, Y. B. Yao, B. J. Wang, B. B. Zhang, L. Li, and Y. C. Wang, Opt. Express **21**, 8701 (2013).
20. Y. H. Hong, Opt. Express **21**, 17894 (2013).
21. Z. Q. Zhong, Z. M. Wu, J. G. Wu, and G. Q. Xia, IEEE Photon. J. **5**, 1500409 (2013).
22. J. G. Wu, Z. M. Wu, X. Tang, X. D. Lin, T. Deng, G. Q. Xia, and G. Y. Feng, IEEE Photon. Technol. Lett. **23**, 759 (2011).
23. X. Dou, C. Wu, X. Chen, H. Yin, Q. Zhao, Y. Hao, and N. Zhao, Chin. Opt. Lett. **12**, S10610 (2014).
24. N. Q. Li, W. Pan, S. Y. Xiang, L. S. Yan, L. Bin, X. H. Zou, L. Y. Zhang, and P. H. Mu, IEEE J. Quantum Electron. **48**, 1339 (2012).
25. N. Q. Li, W. Pan, L. S. Yan, B. Luo, X. H. Zou, and S. Y. Xiang, IEEE J. Sel. Top. Quantum Electron. **19**, 0600109 (2013).
26. N. Q. Li, W. Pan, S. Y. Xiang, L. S. Yan, B. Luo, and X. H. Zou, IEEE Photon. Technol. Lett. **24**, 2187 (2012).
27. R. M. Nguimdo, P. Colet, L. Larger, and L. Pesquera, Phys. Rev. Lett. **107**, 034103 (2011).
28. R. M. Nguimdo, M. C. Soriano, and P. Colet, Opt. Lett. **36**, 4332 (2011).
29. A. Argyris, M. Hamacher, K. E. Chlouverakis, A. Bogris, and D. Syvridis, Phys. Rev. Lett. **100**, 194101 (2008).
30. D. Liu, C. Z. Sun, B. Xiong, and Y. Luo, Opt. Express **22**, 5614 (2014).
31. D. A. A. Almanza, A. N. Pisarchik, and F. R. R. Oliveras, IEEE Photon. Technol. Lett. **24**, 605 (2012).
32. G. V. D. Sande, M. C. Soriano, I. Fischer, and C. R. Mirasso, Phys. Rev. E **77**, 055202 (2008).
33. V. S. Udaltsov, L. Larger, J. P. Goedgebuer, A. Locquet, and D. S. Citrin, J. Opt. Technol. **72**, 373 (2005).
34. L. Zunino, M. C. Soriano, I. Fischer, O. A. Rosso, and C. R. Mirasso, Phys. Rev. E **82**, 046212 (2010).
35. M. C. Soriano, L. Zunino, O. A. Rosso, I. Fischer, and C. R. Mirasso, IEEE J. Quantum Electron. **47**, 252 (2011).
36. C. Bandt and B. Pompe, Phys. Rev. Lett. **88**, 174102 (2002).
37. J. P. Toomey and D. M. Kane, Opt. Express **22**, 1713 (2014).
38. M. C. Soriano, V. Flunkert, and I. Fischer, Chaos **23**, 043133 (2013).
39. R. M. Nguimdo, R. Tchitnga, and P. Woafo, Chaos **23**, 043122 (2013).